Engineering 4 (2018) 869–880

Contents lists available at ScienceDirect

Engineering

journal homepage: www.elsevier.com/locate/eng

Research
Robotics—Article

Design of a Lightweight Force-Feedback Glove with a Large Workspace

Yukai Zheng [a], Dangxiao Wang [a,b,*], Ziqi Wang [a], Yu Zhang [a], Yuru Zhang [a,b], Weiliang Xu [c]

[a] State Key Laboratory of Virtual Reality Technology and Systems, Beihang University, Beijing 100083, China
[b] Beijing Advanced Innovation Center for Biomedical Engineering, Beihang University, Beijing 100083, China
[c] Department of Mechanical Engineering, University of Auckland, Auckland 1142, New Zealand

ARTICLE INFO

Article history:
Received 12 March 2018
Revised 25 June 2018
Accepted 23 October 2018
Available online 30 October 2018

Keywords:
Force-feedback glove
Lightweight
Large workspace
Pneumatic
Virtual reality

ABSTRACT

A wearable force-feedback glove is a promising way to enhance the immersive sensation when a user interacts with virtual objects in virtual reality scenarios. Design challenges for such a glove include allowing a large fingertip workspace, providing a desired force sensation when simulating both free- and constrained-space interactions, and ensuring a lightweight structure. In this paper, we present a force-feedback glove using a pneumatically actuated mechanism mounted on the dorsal side of the user's hand. By means of a triple kinematic paired link with a curved sliding slot, a hybrid cam-linkage mechanism is proposed to transmit the resistance from the pneumatic piston rod to the fingertip. In order to obtain a large normal component of the feedback force on the user's fingertip, the profile of the sliding slot was synthesized through an analysis of the force equilibrium on the triple kinematic paired link. A prototype five-fingered glove with a mass of 245 g was developed, and a wearable force-measurement system was constructed to permit the quantitative evaluation of the interaction performance in both free and constrained space. The experimental results confirm that the glove can achieve an average resistance of less than 0.1 N in free-space simulation and a maximum fingertip force of 4 N in constrained-space simulation. The experiment further confirms that this glove permits the finger to move freely to simulate typical grasping gestures.

1. Introduction

A force-feedback glove is a type of wearable haptic device that allow users to touch and manipulate virtual objects in an intuitive and direct way via the dexterous manipulation and sensitive perception capabilities of the hands. A high-performance glove is desired in order to provide force and tactile feedback that realistically simulate the touching and manipulation of objects at a high update rate. With the upsurge in virtual reality (VR) and augmented reality (AR) systems in recent years, force-feedback gloves will become an important haptic interface for improving the immersion and interaction characteristics of VR systems.

Many force-feedback gloves have been developed in the last three decades, most of which are research prototypes [1–7]; only a few are commercially available for developing VR applications [8]. Unfortunately, none of these existing gloves can meet the stringent performance requirements of ideal force feedback for VR interaction. First, the gloves are not light enough. Based on the success of desktop force-feedback devices such as the PHANTOM Desktop device [9], the equivalent mass of a device should be less than 100 g in order for users to experience an intangible free-space sensation. Second, the gloves should have a large motion range in order to simulate typical grasping positions, and a large force and impedance range in order to simulate interactions in constrained space. Third, the gloves should be easy to put on and remove, and should be adaptable for users with different hand sizes.

In this paper, we present a force-feedback glove using a pneumatically actuated mechanism in order to meet the contradictory requirements of free-space simulation and constrained-space simulation. The contributions of the proposed work include the following:

(1) We propose a novel and simple force-transmission solution using a hybrid cam-linkage mechanism. Using a triple kinematic paired link with a higher cam pair, the mechanism is not only able to transmit resistance forces from a pneumatic piston rod to the user's fingertip, but is also lightweight. A systematic model to derive the profile of the curved sliding slot on the triple-paired link

* Corresponding author.
E-mail address: hapticwang@buaa.edu.cn (D. Wang).

https://doi.org/10.1016/j.eng.2018.10.003

is introduced by means of force equilibrium in order to achieve a large normal component of the feedback force on the fingertip for any given configuration of the finger joints.

(2) A large workspace is obtained for the fingertip by mounting the mechanism on the dorsal side of the user's hand. The geometric shape of the triple-paired link was designed based on the envelope profile of the fingers for different rotating configurations; as a result, this mounting solution allows the full-closure motion of the fingers without interference between the link and the hand.

(3) A wearable force-measurement solution is proposed in order to quantitatively evaluate the performance of the glove in free space and in constrained space. The experimental results demonstrate that the proposed transmission solution greatly reduces the mass of the moving links and the friction force in the kinematic pairs; thus, it achieves a good back-drivability for simulating a free-space sensation with an average resistance force of less than 0.1 N. To simulate a constrained-space sensation, the transmission mechanism provides a large normal component of the feedback force with a maximum of 4 N, while the force measured in the direction tangential to the fingertip is smaller than 0.5 N for most finger configurations.

The remainder of this paper is organized as follows. In Section 2, we review related works on existing force-feedback gloves. In Section 3, we propose a mechanical design solution, with a focus on the design of the mechanism with a curved sliding slot. In Section 4, we elaborate the control system design. Section 5 contains experimental results and Section 6 contains discussions. These are followed by conclusions and future work in Section 7.

2. Related works

There are two types of actuation solutions for force-feedback gloves: passive and active actuation. Passive actuated gloves use a brake, controllable damper, or electromagnetic clutch to provide resistance forces [3,4,10,11]. Users can feel the resistance when the passive actuator is engaged. Passive actuations never harm the user, even in the event of system failure. However, they cannot provide force feedback when the user's hand remains motionless; therefore, they are unable to achieve active force feedback or render variable stiffness.

Active actuations such as electric motors [1,2,4,12] and pneumatics [13–15] have been widely used in force-feedback gloves. The advantage of an active actuation solution is that it can provide active control and simulate active force and motion output at a high update rate; its disadvantage lies in the potential risk of injuring the fingers in the event of a system failure. To avoid potential injury, most active haptic gloves limit the maximum output force to approximately 10 N.

Along with the type of actuation solution, transmission and kinematics are important issues when designing a force-feedback glove. The design becomes a tradeoff problem that includes selecting the number of actuators and designing the transmission mechanism, and thus obtaining a balance between the simplicity of the mechanism and the fidelity of the feedback force.

First, the number of actuators is an important parameter to consider when designing a force-feedback glove. In order to provide three-dimensional (3D) force feedback on a fingertip, a fully actuated solution may require three actuators on each finger, which means fifteen actuators for a five-fingered force-feedback glove. Therefore, a fully actuated solution may result in a heavy weight and a high cost. As a result, such solutions have been rarely used in existing gloves. Under-actuated solutions are common; for example, one electric motor is used to provide feedback force for each finger in the CyberGrasp device [8], and one piston rod is used to provide resistance force for each finger in the RMII-ND glove [13].

After the number of actuators has been determined, the design of the transmission mechanism is the key to achieving the desired performance of a haptic glove. As the actuator is normally fixed on the palm or the wrist, and the fingertip moves along a complex spatial trajectory with respect to the wrist, a mechanism is needed to transmit the torque of the actuator to the end-effectors mounted on the fingertip of the user.

One of the difficulties in designing a transmission mechanism is the need to consider the apparently contradictory requirements of the free-space simulation and the constrained-space simulation. From one perspective, the weight and inertia of the links in the mechanism should be small, and the friction force in each kinematic pair should be low. This makes it possible to achieve satisfactory back-drivability in order to simulate free-space sensation. From the other perspective, the strength and stiffness of the links should be considerable in order to provide a sufficient range of force feedback and an overall high degree of stiffness for the constrained-space simulation. Furthermore, in order to reduce error accumulation in the accuracy of the feedback force, which is caused by the transmission mechanism, it is desirable to use a mechanism with few links and kinematic pairs.

Among the various solutions for the design of transmission mechanisms, cable-driven transmission systems are widely used in force-feedback gloves [2,8,12]. Cable-driven solutions have the obvious advantages of small inertia, long distance transmission, and no backlash. However, specially designed mechanical assembly and control algorithms are needed to maintain the cable's tension and thus ensure the performance of a cable-driven system [16].

Last but not least, it remains a challenge to quantitatively evaluate the performance of force-feedback gloves. For desktop force-feedback devices such as the PHANTOM Desktop [9] and the omega.3 [17], detailed performance metrics such as the maximal stiffness in constrained space and the equivalent resistance force in free space can be provided. However, for force-feedback gloves, very few systems provide quantified performance data. For example, for the CyberGrasp device [8], quantified data are unavailable for the back drivability and the maximal stiffness. Similarly, the simulated maximal stiffness of the Rutgers Master II-New Design (RMII-ND) glove is not available. The main reason for the absence of such quantified data is the lack of an evaluation system that can simultaneously measure the real-time motion and the feedback force during users' manipulation of a force-feedback glove.

3. Design of the hybrid cam-linkage mechanism

3.1. Concept design

As shown in Fig. 1, our proposed hybrid cam-linkage mechanism is fixed on the user's palm. Ignoring the abduction/adduction motion of the proximal joint, the whole kinematic system including the mechanism and the finger can be considered to be a planar mechanism. Compressed air is injected into a pneumatic cylinder (link 7), which exerts resistance force on a piston rod (link 6). One transmission link (i.e., link 4 or the cam) consisting of three kinematic pairs (tuning pair F, tuning pair D, and a higher cam pair, H) is utilized to transmit the actuated force from the rod to the fingertip. As the trajectory of the fingertip is a curve, a curved sliding slot within the triple-paired link (link 4) is introduced. When the finger moves, a disc (link 5) slides along the slot and rotates against the palm through a tuning kinematic pair (pair G).

Excluding the user's finger, the number of degrees of freedom (DOF) of the planar mechanism is defined as $F = 3n - 2P_L - P_H - F_P$, where n, P_L, P_H, and F_P refer to the number of moving links, number of lower kinematic pairs, number of higher kinematic pairs, and number of partial DOF, respectively.

In the proposed mechanism, $n = 4$, $P_L = 4$, $P_H = 1$, and $F_P = 1$. As the number of DOFs of the planar mechanism is 2, the mechanism is able to support any arbitrary movement of the fingertip in the flexion-extension plane.

One feature of the proposed mechanism is that it can fulfill the force-transmission requirement using only one transmission link (link 4). This allows the weight of the force-feedback glove to be greatly reduced. Another important feature is that the designed linkage was not intended for producing an arbitrary 3D force on the fingertip. Instead, by designing a specific profile of the curved sliding slot on the triple-paired link, the proposed mechanism can provide a large normal force with a negligible tangential force on the user's fingertip. We elaborate this issue in Section 3.2.

In Section 3.3, the inverse force model is derived in order to compute the required air pressure for a given feedback force on the fingertip. A large fingertip workspace is obtained by mounting the mechanism on the dorsal side of the user's hand. In Section 3.4, the geometric shape of the triple-paired link is appropriately determined in order to ensure that no interference occurs between the mechanism and the hand.

3.2. Profile of the curved sliding slot

As only one piston rod is used to provide resistance forces, the design goal of the mechanism is to obtain as much of a normal component of the feedback force on the fingertip as possible for any finger configurations. In the proposed mechanism, the curved profile of the sliding slot is the key to achieving this goal and to ensuring the free movement of the finger joints.

In this paper, we synthesize the profile in two steps by analyzing the motion and force characteristics of the mechanism. First, we utilize the mapping between the sampling points along the fingertip trajectory and the corresponding reference points along the profile of the sliding slot. Second, in order to obtain a negligible tangential force on the fingertip, we construct force-equilibrium equations that dictate the relationship between the normal feedback force on the fingertip and the tangential direction of the slot at each reference point.

In the first step, the design rationale is that for a given motion sequence of the fingertip, the profile of the sliding slot can be defined by several reference points at corresponding locations. Fig. 2 shows the sampling points (P_1–P_7) along the fingertip trajectory and the corresponding reference points along the profile of the sliding slot.

Therefore, we formulate the problem of synthesizing the profile as follows: Given the length of all links and the trajectory of the fingertip (defined by the combination of the rotating angle of the finger joints), we need to determine the profile of the curved slot. To explore this problem, as shown in Table 1, we define seven sampling points along the trajectory of the fingertip. In this Table, θ_1, θ_2, and θ_3 refer to the rotation angle of the three joints from the

Table 1
Sampling points along the trajectory of the fingertip.

Index	Fingertip	θ_1 (°)	θ_2 (°)	θ_3 (°)
1	P_1	−15	0	0
2	P_2	0	0	0
3	P_3	0	20	0
4	P_4	10	35	10
5	P_5	25	45	25
6	P_6	30	50	35
7	P_7	35	60	40

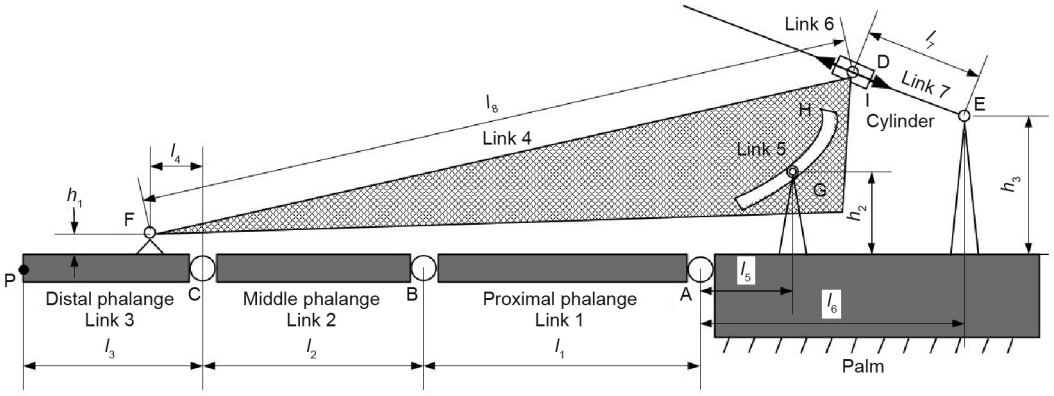

Fig. 1. A kinematics diagram of the hybrid cam-linkage mechanism on a user's index finger.

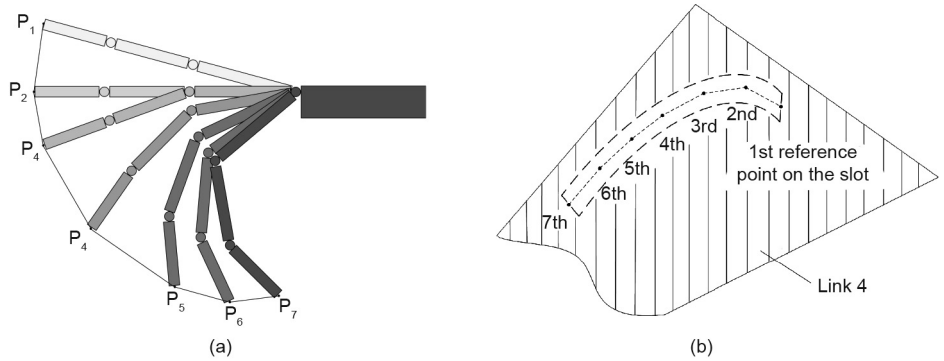

Fig. 2. Mapping from the fingertip motion to the profile of the curved sliding slot. (a) Sampling points (P_1–P_7) along the fingertip trajectory; (b) corresponding reference points along the profile of the sliding slot.

proximal to the distal end of the finger. The coordinate systems are defined as shown in Fig. 3. All the coordinate frames are defined in a right-handed style.

For each of the seven sampling points in Table 1, we aim to compute the corresponding reference point (^6P_G) on the profile of the curved sliding slot—that is, to compute the coordinate of point G with respect to the coordinate frame O_6. Based on the kinematic diagram in Fig. 1, the following homogeneous equations can be constructed:

$$\begin{cases} {}^6P_F = {}^6T_5{}^5T_4{}^4T_0{}^0T_1{}^1T_2{}^2T_3{}^3P_F = [l_8\ 0\ 0]^T \\ {}^0P_G = {}^0T_4{}^4T_5{}^5T_6{}^6P_G = [-l_5\ \ -h_2\ 0]^T \end{cases} \tag{1}$$

In Eq. (1), ${}^mT_n$ is the matrix which can transform a point from coordinate frame O_n to coordinate frame O_m. These equations contain five unknown variables, ${}^6P_{G\_x}$, ${}^6P_{G\_y}$, l_7, θ_5, and θ_6, while all the other parameters, l_1, l_2, l_3, l_4, l_5, l_6, l_8, θ_1, θ_2, θ_3, h_1, and h_2, are known. Using these equations, the coordinate of point F can be described as $[l_8\ 0\ 0]^T$ with respect to the coordinate frame O_6, and point G can be described as $[-l_5\ \ -h_2\ 0]^T$ in the same way.

As we only consider the components along the x-axis and the y-axis in the coordination system, we can derive four equations from Eq. (1). Therefore, we need another equation to solve the five unknown variables. Here, we propose a fifth equation using the tangential direction along the profile of the curved sliding slot. If we describe the curve as $y = f(x)$, according to the characteristic of the cam, the tangent of the curve at every reference point is always perpendicular to the direction of fingertip feedback force $\boldsymbol{F}_3$, as follows:

$$\frac{\partial y}{\partial x} \perp \boldsymbol{F}_3 \tag{2}$$

As shown in Fig. 4, at each reference point of the curved profile, we can construct a tangential line. Thus, we can obtain Eq. (3) using discrete point coordinates on the curve in order to approximately solve Eq. (2).

$$\frac{(p_{i\_x} - p_{i-1\_x})}{(p_{i\_y} - p_{i-1\_y})} - \frac{(p_{i\_x} - p_x^*)}{(p_{i\_y} - p_y^*)} = 0 \tag{3}$$

where p_{i-1_x} and p_{i-1_y} denote the x and y components of the previous reference point on the profile, and p_{i_x} and p_{i_y} denote the x and y components of the next reference point on the profile, which are the two unknown variables in this equation. p_x^* and p_y^* denote the x and y components of the tangential vector ${}^6\boldsymbol{P}_{dir}$, which is perpendicular to the vector $\boldsymbol{F}_3$. This equation shows that the desired curve is always perpendicular to the vector $\boldsymbol{F}_3$ in the static state. By combining Eqs. (1) and (3), we obtain the five unknown variables ${}^6P_{G\_x}$, ${}^6P_{G\_y}$, l_7, θ_5, and θ_6. It should be noted that when we calculate the first reference point on the curve, there is a slight difference in Eq. (2). Because $\partial y/\partial x$ is unknown at this time, we cannot construct the fifth equation, which means that there are only four equations. Thus, we set ${}^6P_{G\_y}$ as a known variable so that four unknown variables remain. Next, we can calculate the coordinates of the first reference point.

In order to construct Eq. (3), it is necessary to know the direction of the line between each pair of adjacent sampling points—that is, the vector $\boldsymbol{P}_{dir}$. As shown in Fig. 4, this vector is approximately perpendicular to the vector $\boldsymbol{F}_3$.

$$\boldsymbol{P}_{dir} = \begin{bmatrix} \cos(\pi/2) & -\sin(\pi/2) & 0 \\ \sin(\pi/2) & \cos(\pi/2) & 0 \\ 0 & 0 & 1 \end{bmatrix} \boldsymbol{F}_3 \tag{4}$$

As shown in Fig. 5, the direction of fingertip feedback force $\boldsymbol{F}_3$ can be determined by the force-equilibrium and torque-equilibrium equations for the triple-paired link (i.e., the shaded link in Fig. 5). The following equations can be derived for point G:

$$\begin{cases} \boldsymbol{F}_3 + \boldsymbol{F}_1 + \boldsymbol{F}_2 = 0 \\ \boldsymbol{F}_1 \times \boldsymbol{L}_1 + \boldsymbol{F}_2 \times \boldsymbol{L}_2 = 0 \end{cases} \tag{5}$$

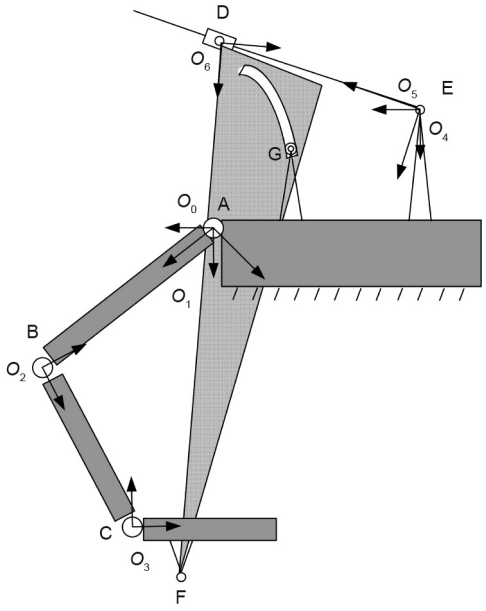

Fig. 3. Definition of the coordinate frames. All the letters "O" designates a coordinate frame.

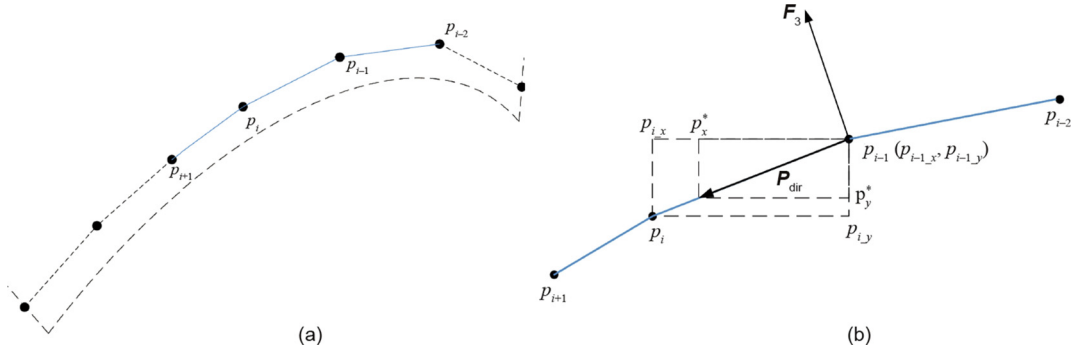

Fig. 4. Construction of the tangential line at each reference point along the curved profile. (a) The tangential lines at each of the seven reference points; (b) an enlarged view of a tangential line at one reference point.

where $\boldsymbol{L}_1$ denotes the vector from F to G in coordinate frame O_6, and $\boldsymbol{L}_2$ denotes the vector from D to G in coordinate frame O_6.

After solving the profile using Eqs. (1) and (3), we obtained the seven reference points along the profile, which are shown in Fig. 6(a). A turning point appears at the 4th point, which implies that for a given trajectory of the fingertip, the motion of slider 5 is not unidirectional, but bi-directional. If we were to manufacture the sliding slot based on this result, the slot would have two branches to allow a back-and-forth motion of the slider. The mechanical structure would be complex and the friction force at the turning point would be great.

To solve this problem, we propose a simplified profile. As shown in Fig. 2(a), the rotating angles of the finger joints become very big when the finger joints rotate beyond the 4th sampling point. These finger configurations (i.e., the 5th, 6th, and 7th sampling points) are not used very frequently in daily manipulations. Therefore, we simplify the profile by removing the last three reference points. Instead, we use a linear interpolation to produce another new point as the fifth reference point. Finally, using a spline-fitting algorithm, we formulate a new profile as shown in Fig. 6(b). The experimental data in Section 6 demonstrate that this simplified profile can ensure free motion of the fingertip, and can transmit the resistance force from the rod to the fingertip.

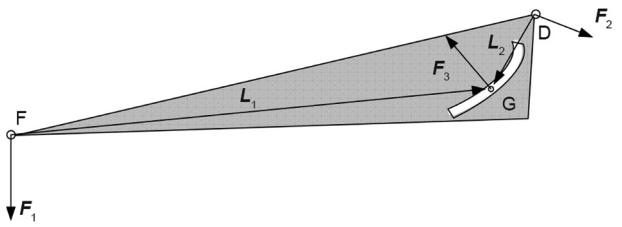

Fig. 5. An illustration of the force-equilibrium principle for the triple-paired link.

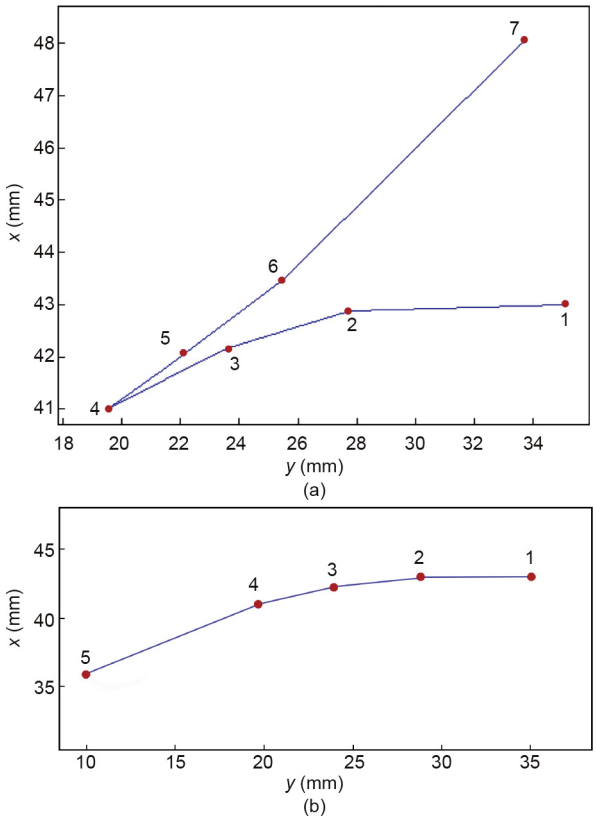

Fig. 6. Reference points on the profile of the slot. (a) Original reference points computed by the model; (b) new profile using simplification and spline fitting.

3.3. Inverse force model

As shown in Fig. 5, the role of the inverse force model is to compute the required resistance force, $\boldsymbol{F}_2$, on the piston rod when a specified fingertip force $\boldsymbol{F}_1$ is required; that is:

$$\boldsymbol{F}_2 = g(\boldsymbol{F}_1) \tag{6}$$

where g is a function. It should be noted that this equation is dependent on the configuration of the finger joints—that is, on the combination of the finger joint angles.

The computation model includes the following four steps:

Step 1: Compute the position, ${}^6P_G$, of the slider (i.e., link 5) on the curved profile, based on the given combination of the three joint angles.

Given the combination of the three joint angles, the distance between points F and G can be derived as follows:

$$L_{FG} = \sqrt{\left({}^0P_{FG\_x}\right)^2 + \left({}^0P_{FG\_y}\right)^2} \tag{7}$$

where

$${}^0P_{FG} = {}^0P_F - {}^0P_G \tag{8}$$

where

$$\begin{cases} {}^0P_F = {}^0T_1\,{}^1T_2\,{}^2T_3\,{}^3P_F \\ {}^0P_G = [-l_5 \;\; -h_2 \;\; 1]^T \end{cases} \tag{9}$$

and

$${}^3P_F = [l_4 \;\; -h_1 \;\; 1]^T \tag{10}$$

By comparing the distance between points F and G, which is L_{FG}, with the distance from point F to the five reference points, which is D_i, on the curved profile, we can determine the position of an arbitrary point on the profile—for example, when $D_i < L_{FG} < D_{i+1}$, this can be done by using the linear interpolation between the reference points by means of the following equations:

$$\begin{cases} {}^6P_{G\_x} = p_{i\_x} + k(p_{i+1\_x} - p_{i\_x}) \\ {}^6P_{G\_y} = p_{i\_y} + k(p_{i+1\_y} - p_{i\_y}) \end{cases} \tag{11}$$

where

$$k = (L_{FG} - D_i)/(D_{i+1} - D_i) \tag{12}$$

Step 2: Compute the direction of force $\boldsymbol{F}_3$—that is, $\boldsymbol{F}_{3\_dir}$.

$$\boldsymbol{F}_{3\_dir} = \begin{bmatrix} \cos(\pi/2) & -\sin(\pi/2) & 0 \\ \sin(\pi/2) & \cos(\pi/2) & 0 \\ 0 & 0 & 1 \end{bmatrix} \begin{bmatrix} p_{i+1\_x} - p_{i\_x} \\ p_{i+1\_y} - p_{i\_y} \\ 0 \end{bmatrix} \tag{13}$$

Step 3: Compute the direction of force $\boldsymbol{F}_2$—that is, $\boldsymbol{F}_{2\_dir}$.

$$\begin{cases} {}^6P_G = {}^6T_5\,{}^5T_4\,{}^4T_0\,{}^0P_G \\ {}^6P_F = {}^6T_5\,{}^5T_4\,{}^4T_0\,{}^0T_1\,{}^1T_2\,{}^2T_3\,{}^3P_F \end{cases} \tag{14}$$

Therefore

$$\boldsymbol{F}_{2\_dir} = {}^6T_5\,{}^5\boldsymbol{F}_{2\_dir} \tag{15}$$

where

$${}^5\boldsymbol{F}_{2\_dir} = [1 \;\; 0 \;\; 0]^T \tag{16}$$

and

$${}^6T_5 = \begin{bmatrix} \cos\theta_6 & \sin\theta_6 & -l_7\cos\theta_6 \\ -\sin\theta_6 & \cos\theta_6 & l_7\sin\theta_6 \\ 0 & 0 & 1 \end{bmatrix} \tag{17}$$

Step 4: Compute the magnitude of force $\boldsymbol{F}_2$, based on the force-equilibrium principle for the triple-paired link.

We then construct force and torque equilibrium equations as per Eq. (5). In addition,

$$\begin{cases} \boldsymbol{F}_2 = k_2 \boldsymbol{F}_{2\_\mathrm{dir}} \\ \boldsymbol{F}_3 = k_3 \boldsymbol{F}_{3\_\mathrm{dir}} \end{cases} \tag{18}$$

where k_2 denotes the magnitude of $\boldsymbol{F}_2$ and k_3 denotes the magnitude of $\boldsymbol{F}_3$.

Regarding the constructed force and torque equilibrium equations, there are three equations, three known variables (i.e., $\boldsymbol{F}_1$, $\boldsymbol{F}_2$, and $\boldsymbol{F}_3$), and three unknown variables (i.e., k_2, k_3, and F_{1t}, the magnitude of the tangential component of $\boldsymbol{F}_1$).

Based on the geometric relationship in Fig. 3, we derive the following:

$${}^6F_1 = {}^6T_5{}^5T_4{}^4T_0{}^0T_1{}^1T_2{}^2T_3{}^3F_1 \tag{19}$$

Because ${}^3F_1 = [F_{1t}\ F_{1n}\ 0]$, where F_{1n} denotes the magnitude of the normal component of $\boldsymbol{F}_1$, we can derive the following:

$${}^6F_1 = [\beta \cdot F_{1t} - \alpha \cdot F_{1n} \quad \alpha \cdot F_{1t} + \beta \cdot F_{1n} \quad 0]^{\mathrm{T}} \tag{20}$$

where

$$\begin{cases} \alpha = \sin(\theta_1 + \theta_2 + \theta_3 - \theta_5 - \theta_6) \\ \beta = \cos(\theta_1 + \theta_2 + \theta_3 - \theta_5 - \theta_6) \end{cases} \tag{21}$$

Therefore, we can compute the magnitude of $\boldsymbol{F}_2$ as follows:

$$k_2 = F_{1n}(A + B)/(C + D) \tag{22}$$

where

$$\begin{cases} A = \dfrac{\alpha \cdot {}^6L_{1\_y} + \beta \cdot {}^6L_{1\_x}}{\beta \cdot {}^6L_{1\_y} - \alpha \cdot {}^6F_{2\_\mathrm{dir}\_x}} \left(\dfrac{\beta}{{}^6F_{3\_\mathrm{dir}\_x}} - \dfrac{\alpha}{{}^6F_{3\_\mathrm{dir}\_y}} \right) \\ B = \left(\dfrac{\alpha}{{}^6F_{3\_\mathrm{dir}\_x}} + \dfrac{\beta}{{}^6F_{3\_\mathrm{dir}\_y}} \right) \\ C = \left(\dfrac{{}^6F_{2\_\mathrm{dir}\_x}}{{}^6F_{3\_\mathrm{dir}\_x}} - \dfrac{{}^6F_{2\_\mathrm{dir}\_y}}{{}^6F_{3\_\mathrm{dir}\_y}} \right) \\ D = \dfrac{{}^6F_{2\_\mathrm{dir}\_x}{}^6L_{2\_y} - {}^6F_{2\_\mathrm{dir}\_y}{}^6L_{2\_x}}{\beta \cdot {}^6L_{1\_y} - \alpha \cdot {}^6L_{1\_x}} \left(\dfrac{\beta}{{}^6F_{3\_\mathrm{dir}\_x}} - \dfrac{\alpha}{{}^6F_{3\_\mathrm{dir}\_y}} \right) \end{cases} \tag{23}$$

Furthermore, we can compute the magnitude of the tangential component of $\boldsymbol{F}_1$ as follows:

$$F_{1t} = \frac{\alpha \cdot {}^6L_{1\_y} + \beta \cdot {}^6L_{1\_x} + k_2 \left({}^6F_{2\_\mathrm{dir}\_x} \cdot {}^6L_{2\_y} - F_{2\_\mathrm{dir}\_y} \cdot {}^6L_{2\_x} \right)}{\beta \cdot {}^6L_{1\_y} - \alpha \cdot {}^6L_{1\_x}} \tag{24}$$

where

$$\begin{cases} {}^6L_1 = {}^6T_5{}^5T_4{}^4T_0{}^0P_{\mathrm{G}} - {}^6P_{\mathrm{F}} \\ {}^6L_2 = {}^6T_5{}^5T_4{}^4T_0{}^0P_{\mathrm{G}} - {}^6P_{\mathrm{D}} \end{cases} \tag{25}$$

3.4. Structural design

In the proposed mechanism, it is important to determine the shape of the triple-paired link. This link should allow the fingers to perform various grasping movements. In order to prevent the linkage from interfering with the hand when the user rotates the finger joints, the shape of the triple-paired link was determined by drawing the envelope profile of the hand when the fingers are bent in the configurations shown in Fig. 7(c). As shown in Fig. 7, the designed link can adapt to different rotating angles of the finger joints.

Fig. 8 shows the virtual prototype that was constructed using SolidWorks Program (Dassault Systèmes, France). Iterative design procedures were performed to determine the dimension of each mechanical part in the virtual prototype. In order to guarantee the back-drivability of the glove, specific structural design criteria were adopted, including material selection and dimension optimization. Lightweight material was selected for the links, including carbon fiber for the triple-paired link and plastic materials for the finger cap and the base part that mounts the glove on the user's palm. The triple-paired link was made as thin as possible (i.e., 2 mm) while simultaneously ensuring the necessary stiffness and strength of the link; this reduced the weight.

4. Design of the control system

4.1. Architecture of the control system

The architecture of the control system is shown in Fig. 9. The control system includes a personal computer (PC), a low-level controller, and pneumatic actuation components (i.e., a pneumatic pump, air container, air filter, pressure-reducing valve, electro-pneumatic regulator, pneumatic cylinder, and associated piston rod). (Note that the scheme in Fig. 9 only represents the force feedback for one finger. All five fingers utilize the same control principle.)

The virtual environment and haptic rendering algorithms are run using the PC in order to simulate the virtual grasping operation and produce the commanded feedback force signal. When a user moves his or her hand, the finger motion signals are recorded by the motion-tracking sensors on the glove; these signals can drive a virtual hand avatar in the virtual environment in order to simulate different grasping behaviors.

The low-level controller is a STM32F103 microcontroller with a flash memory of 512 KB, a 12-bit D/A converter, and an operating voltage less than 12 V DC. The controller communicates with the PC through a serial USB port. The controller provides six-channel D/A output signals, which drive the five electro-pneumatic regulators.

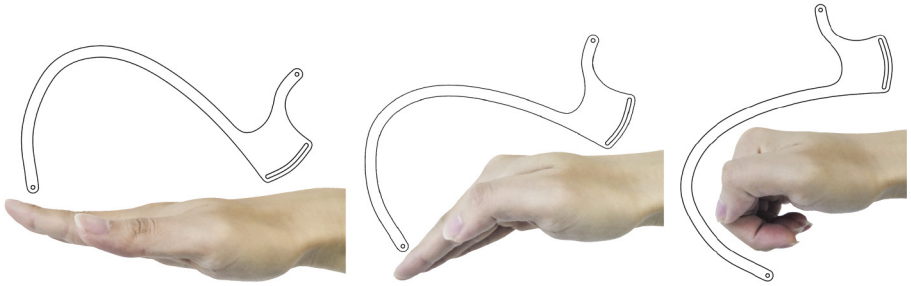

Fig. 7. The curved shape of the link adapts to different rotating angles of the fingers. (a) Fingers stretching; (b) small rotation; (c) large rotation.

The function of the pneumatic pump is to produce compressed air; the air container then consistently maintains the air pressure above a threshold value in order to avoid frequent pump on and offs. The function of the air filter is to eliminate oil contamination in the air and thus prolong the lifespan of the regulator. The pressure-reducing valve stabilizes the air pressure input to the regulator, and the electro-pneumatic regulator produces controllable pressure input into the pneumatic cylinder.

Each electro-pneumatic regulator is connected to the first port (Port 1) of a double-acting cylinder. The other port of the cylinder is open to the ambient air. The friction force between the piston rod and the cylinder is small enough to ensure a smooth movement of the rod in order to simulate free space. To simulate constrained space, the air pressure inflated into the cylinder creates resistance forces on the piston rod; these forces are transmitted to the user's fingers through the linkage mechanism.

4.2. Modeling force control

The performance metrics for simulating constrained space include the maximum feedback force exerted on the fingertip, the resolution of the feedback force, the responsiveness of the force feedback, and the maximal stiffness that can be rendered by the glove.

The magnitude of the actuated force on the piston rod is determined by the following:

$$\|\boldsymbol{F}_2\| = P_{\mathrm{d}}\left(\pi R^2 - \pi r^2\right) - P_0 \pi R^2 \tag{26}$$

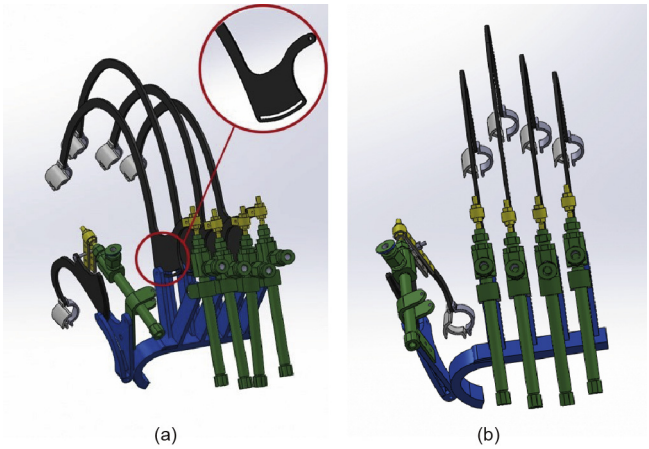

Fig. 8. A virtual prototype of the force-feedback glove created using SolidWorks Program.

where P_{d}, P_0, πR^2, and πr^2 denote the air pressure inflated into the cylinder, the ambient air pressure, the cross-sectional area of the pneumatic cylinder, and the cross-sectional area of the piston rod, respectively.

The pressure range was determined by the tradeoff between the required maximal force on the fingertip and the constraint of keeping the glove lightweight. On the one hand, a larger pressure can result in a large fingertip force. On the other hand, a larger pressure requires a bigger pneumatic cylinder, which may increase the weight of the glove. Therefore, the upper limit of the pressure is constrained by the weight and size of the cylinder. The pressure was computed using Eqs. (6) and (26) in order to obtain the required force on the fingertip.

Based on the model of the electro-pneumatic regulator, the following can be derived:

$$P_{\mathrm{d}} = k_{\mathrm{r}} U_{\mathrm{r}} \tag{27}$$

where U_{r} denotes the voltage input to the electro-pneumatic regulator and k_{r} denotes the coefficient of the electro-pneumatic regulator.

Combining Eqs. (26) and (27) allows the maximum force exerted on the piston rod to be computed; this is determined by the maximal output voltage of the regulator. Using the following forward force model, the maximum force exerted on the fingertip can be computed:

$$\boldsymbol{F}_1 = J^{\mathrm{T}} \boldsymbol{F}_2 \tag{28}$$

where J denotes the Jacobin matrix, which is dependent on the configuration of the finger joints.

Furthermore, it is possible to compute the force resolution of the exerted force on the fingertip ($\Delta \boldsymbol{F}_1$) as follows:

$$\Delta \boldsymbol{F}_1 = J^{\mathrm{T}} \Delta \boldsymbol{F}_2 \tag{29}$$

where $\Delta \boldsymbol{F}_2$ denotes the force resolution of the exerted force on the piston rod, which can be computed by differentiating the force model in Eq. (28). Ultimately, the force resolution is determined by the voltage resolution of the regulator.

As shown in Fig. 7, the responsiveness of the glove is quantified by the delay from the onset of the commanded force signal produced by the virtual environment to the feedback force exerted on the user's fingertip. The delay can be roughly modeled as follows:

$$\Delta T_{\mathrm{d}} = \Delta T_1 + \Delta T_2 + \Delta T_3 + \Delta T_4 + \Delta T_5 \tag{30}$$

where ΔT_1 denotes the communication delay from the personal computer (PC) to the controller, which is determined by the communication hardware and protocol; ΔT_2 denotes the delay from the controller to the pump, which is determined by the type of

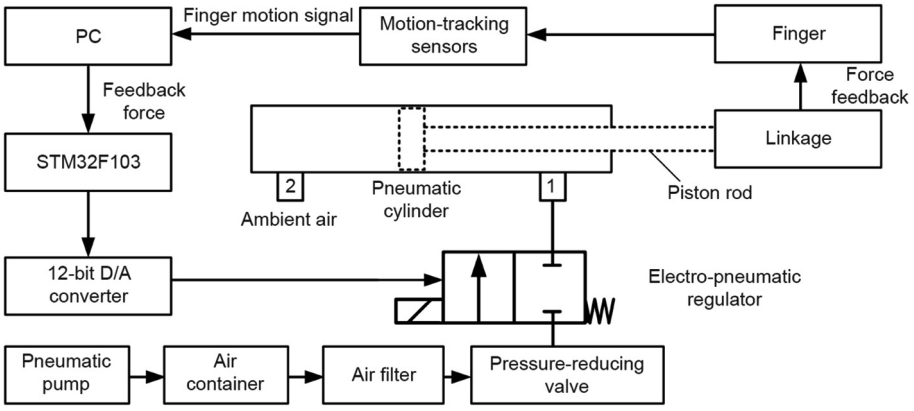

Fig. 9. Architecture of the control system.

controller and the update rate of the timer in the controller; and ΔT_3 denotes the delay from the pump to the electro-pneumatic regulator, which is determined by the dynamic response of the pump. In this paper, we utilized a buffered air container and a pump, which conserve the air pressure and thus eliminate the delay. ΔT_4 denotes the delay from the regulator to the cylinder, which is determined by the airflow velocity in the air tube. The velocity is influenced by the diameter and length of the tube. ΔT_5 denotes the delay from the piston rod to the fingertip.

For a typical virtual wall [18], the simulated stiffness, k_d, rendered by the force-feedback glove can be defined as follows:

$$k_d = \frac{\|\Delta \boldsymbol{F}_1\|}{\|\Delta P_f\|} \tag{31}$$

where ΔP_f denotes the position resolution of the glove for tracking the fingertip motion, and $\Delta \boldsymbol{F}_1$ denotes the force resolution of the exerted force on the fingertip.

4.3. Implementation of the control system

As shown in Table 2, we determined the performance metrics of the main components in the pneumatic system. In order to maintain the back-drivability of the glove to simulate the free-space sensation, the friction force in the sliding pair between the piston rod and the pneumatic cylinder should be as small as possible. Therefore, we selected a piston rod and pneumatic cylinder set with a miniature size and small friction forces. As shown in Table 2, the set is lightweight (26 g) and can support a fairly large output force (19.79 N), while the friction force between the rod and the cylinder is fairly small.

5. Experiments

In this section, we first summarize the major parameters of the physical prototype. Next, we illustrate the workspace of the force-feedback glove. Most importantly, we introduce a measurement method to measure the performance data for simulating the sensations of free space and constrained space. By constructing a wearable force-measurement system, we are able to obtain a quantified evaluation of the glove, including the resistance force on the fingertip during free-space and constrained-space simulation, and the simulated stiffness of the glove.

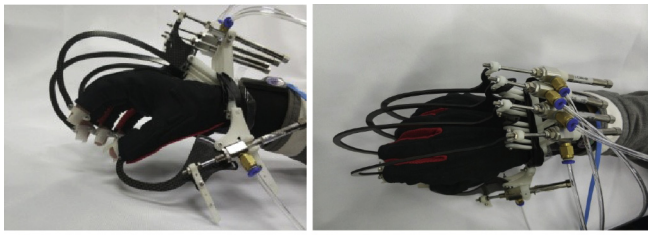

Fig. 10. Physical prototype of the glove. (a) Side view; (b) top view.

5.1. Physical prototype

The physical prototype of the five-finger force-feedback glove is illustrated in Fig. 10. The main characteristics of the force-feedback glove are listed in Table 3. A video clip is provided to illustrate the movement of the glove in both free space and constrained space.

To track the motion of the finger joints, a commercial data glove (WiseGlove, WISEGLOVE Inc., China) in a woven cloth material was adopted. The motion-tracking resolution of the finger joints is 0.02 degrees, and the accuracy of the joint motion measurement is 3 degrees. The sampling rate of the motion signal is 70 Hz.

As shown in Fig. 11, the glove allows free motion of the fingers, including half-closure and full-closure movements. When the hand is moving, there is no interference between the mechanism and the fingers. These results demonstrate that the profile of the curved sliding slot on the triple-paired link is able to allow free motion of the fingers.

When the fingers are in the full-closure position, a minimal virtual sphere with a diameter of 30 mm can be simulated. As shown in Fig. 12, the glove is able to simulate diverse hand positions, include normal grasping and plate-pinching positions.

5.2. Performance evaluation method

A wearable force-measurement system was developed for the quantified evaluation of the performance. The principle of the

Table 2
Performance metrics of the main components in the pneumatic system.

Name	Performance metrics	Type and vendor
Pump	Power: 550 W, volume flow: 40 min^{-1}, nominal discharge pressure: 0.7 MPa	550 W–18 L, TWSNS Inc., China
Air container	Volume: 18 L	550 W–18 L, TWSNS Inc., China
Electro-pneumatic regulator	Pressure range: 0.001–0.9 MPa, linearity: ±1% F.S. or less, sensitivity: 0.2% F.S. or less	ITV0050-2MS, SMC Inc., Japan
Air filter and regulator	Pressure range: 0.05–0.7 MPa, nominal filtration rating: AF: 5 μm, AFM: 0.3 μm, weight: 0.39 kg	AC20C-02BG-A, SMC Inc., Japan
Piston rod and pneumatic cylinder	Weight: 26 g, cylinder standard stroke: 45 mm, maximal force output: 19.79 N	CJ2B6-45R, SMC Inc., Japan

F.S.: full scale; AF: air filter; AFM: mist separator.

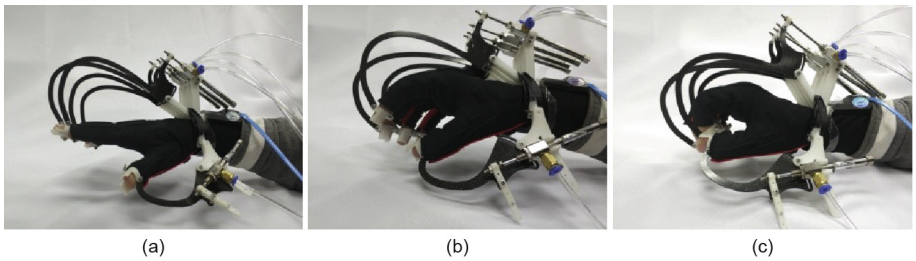

Fig. 11. The capability of the glove to allow free motion. (a) Fingers stretching; (b) half-closure position; (c) full-closure position.

Table 3
Characteristics of the force-feedback glove.

Performance metrics	Value
Weight	245 g
Maximal feedback force on fingertip	4 N
Average resistance force in free space	0.1 N
Number of actuated fingers	Five-finger force-feedback
Response time	130 ms
Workspace	Support full-closure motion
Actuator	Pneumatic cylinder

measurement device is shown in Fig. 13. A customized finger cap was manufactured in order to mount a six-axis force/torque sensor (ATI Nano17, ATI Inc., USA) beneath the fingertip. The fixed end of the force/torque sensor is fixed to the finger cap.

When simulating the sensation of free space, the pneumatic cylinder is powered off. The friction force in the kinematic pairs provides a resistance force during the motion of the user's fingers. This force is transmitted to the fingertip via the finger cap, leading to a relative deformation between the fingertip and the load end of the force/torque sensor. Thus, the measured signals from the force sensor represent the resistance force during free-space simulation.

When simulating the sensation of constrained space, the pneumatic cylinder is powered on. The piston rod transmits a commanded resistance force, F_s, to the finger cap via the mechanism. This force pushes the load end of the sensor and leads to deformation of the fingertip. Thus, the measured signals from the force sensor represent the resistance force during the constrained-space simulation.

The physical prototype of the measurement device is shown in Fig. 14.

5.3. Performance of free-space simulation

Back-drivability is the most important metric to quantify the sensation of free space; it is influenced by the friction force at each kinematic pair, the gravity force and inertial force of each link, and the clearance at each kinematic pair.

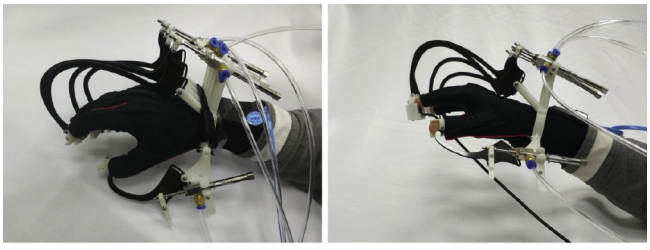

Fig. 12. The capability of the glove to simulate different grasping positions.

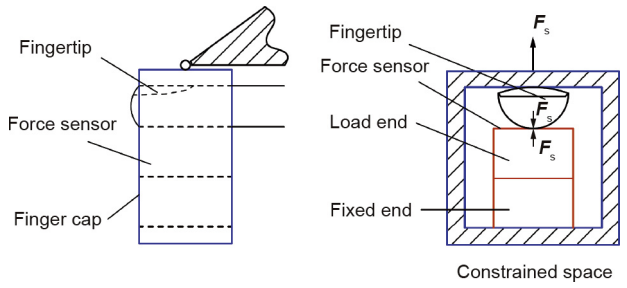

Fig. 13. The principle of the measurement device. (a) Side-view; (b) cross-sectional front view.

Using the proposed measurement system, we measured the resistance force during the free motion of the fingers. The pneumatic cylinder was powered off. A user moved the fingers at a nearly constant velocity (20 mm·s^{-1}) back and forth five times. As shown in Fig. 15, the maximum force was about 0.2 N, and the mean and standard deviation of the resistance force was about (0.068 ± 0.044) N.

5.4. Performance of constrained-space simulation

The performance metrics for constrained space were also measured using the proposed measurement system, including the maximum feedback force exerted on the fingertip, the resolution of the feedback force, the responsiveness of the force feedback, and the maximal stiffness that could be rendered.

As the feedback force on the fingertip is dependent on the configuration of the fingers, we measured the fingertip force at four different configurations. For each configuration, several levels of air pressure were input to the pneumatic cylinder, ranging from 0.1 to 0.55 MPa. (Note that all pressure values given here are relative to the ambient pressure.)

As shown in Fig. 16, with an increase in air pressure, the feedback forces on the fingertip increase linearly. The maximal force was about 4 N for the full-stretch configuration. When the rotation angle of the fingers increased, the maximal force decreased to about 3 N.

Furthermore, with an increase in air pressure, both the theoretical and experimental values of the normal force on the fingertip increased in a similar linear trend; this indicates that the computation model in Eq. (28) is able to roughly predict the fingertip force of the force-feedback glove.

As shown in Table 4, the measured force data in the tangential direction of the fingertip is smaller than 0.8 N for all four configurations. Most of the tangential forces are smaller than 0.5 N. This means that, for the given moving trajectory of the fingertip defined in Fig. 2(a), the hybrid cam-linkage mechanism can provide a much larger component along the normal direction of the fingertip than along the tangential direction of the fingertip. In other words, the proposed profile of the curved slot is able to produce as much normal force as possible on the fingertip. Furthermore, it should be noted that the fourth configuration (45, 0, 0) is not located on the fingertip motion trajectory that was defined by the original seven sampling points. In addition, the force data in the tangential direction is very small for this configuration. This result demonstrates that the slot can adapt to different trajectories of the fingertip.

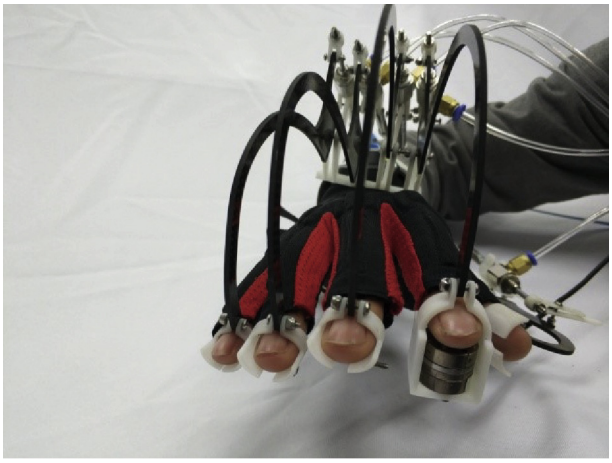

Fig. 14. The physical prototype of the measurement device.

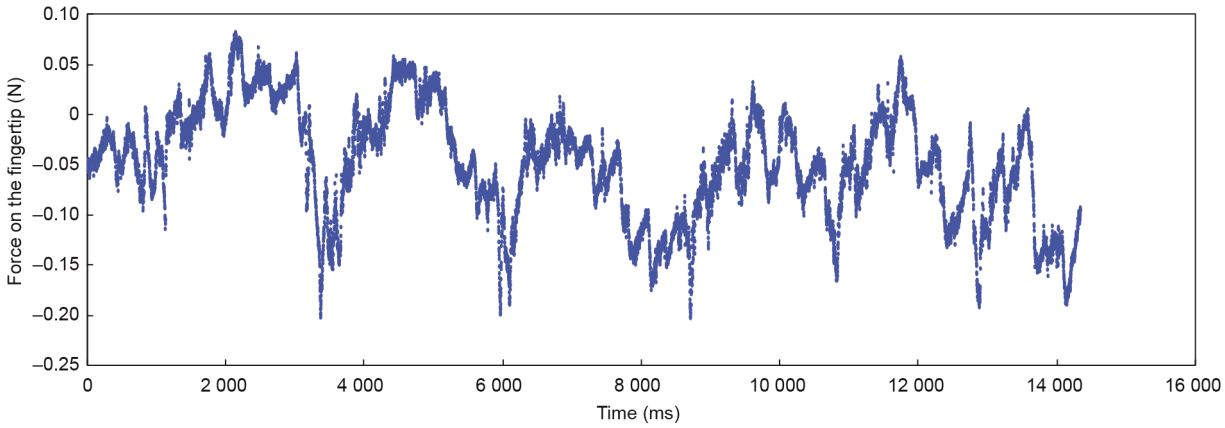

Fig. 15. Normal force signal during the free-space simulation.

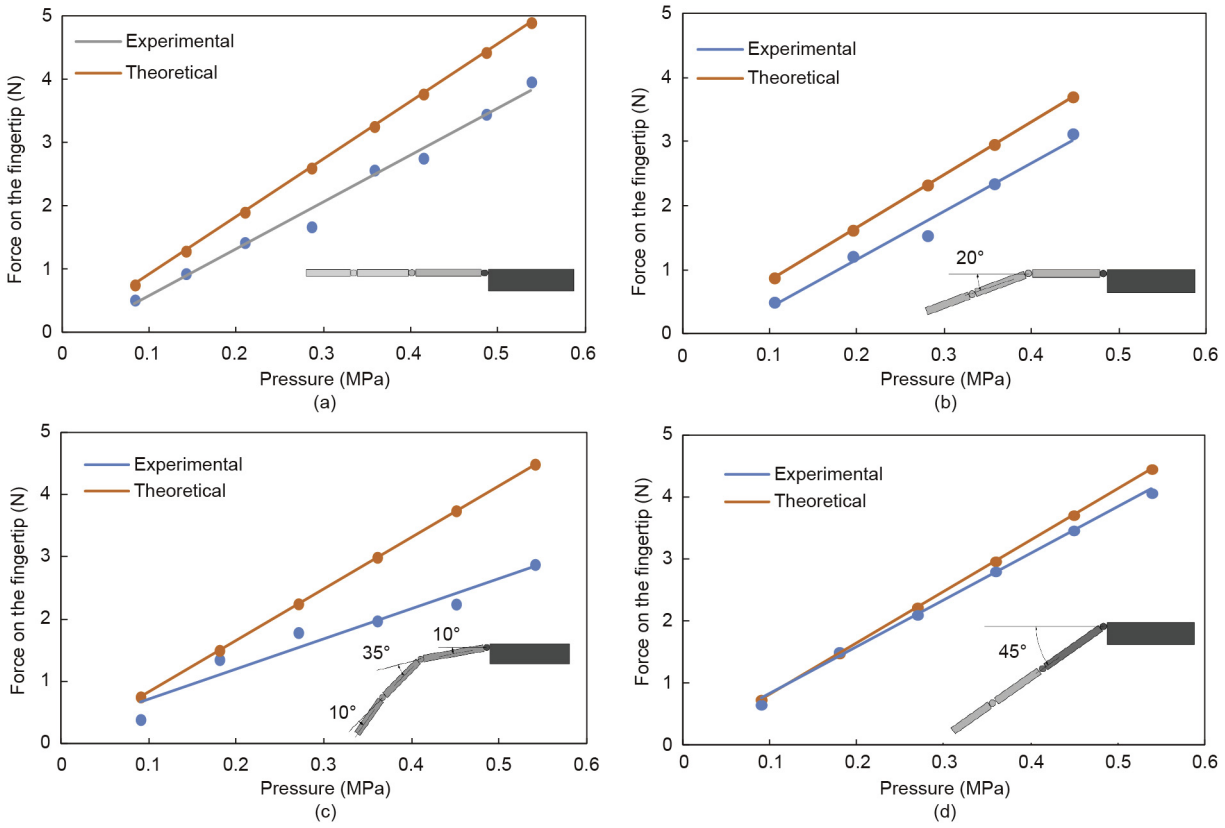

Fig. 16. Normal components of the feedback force on the fingertip under different air pressures. (a) (0, 0, 0) configuration; (b) (0, 20, 0) configuration; (c) (10, 35, 10) configuration; (d) (45, 0, 0) configuration.

Table 4
Tangential components of the feedback force on the fingertip under different air pressures.

Air pressure (MPa)	Feedback force for each configuration (N)			
	(0, 0, 0)	(0, 20, 0)	(10, 35, 10)	(45, 0, 0)
0.09	0.060	0.117	0.265	0.252
0.18	0.248	0.178	0.600	0.242
0.27	0.197	0.276	0.541	0.188
0.36	0.220	0.409	0.464	0.451
0.45	0.247	0.400	0.331	0.355
0.54	0.488	—	0.197	0.787

When combined with the motion-tracking glove, the proposed force-feedback glove can simulate the grasping of virtual objects with different stiffness. For a given virtual wall, the motion trajectory of the fingertip was measured by the motion-tracking glove. We used a spring force model to compute the feedback force on the fingertip. The experimental data show that when the stiffness of the virtual object was 92 $N \cdot m^{-1}$, the user experienced the contact forces as stable and responsive. When the stiffness of the virtual object increased to 138 $N \cdot m^{-1}$, the user felt the stable contact force, but also felt a perceptible delay in force feedback. When the stiffness of the virtual object was greater than 184 $N \cdot m^{-1}$, the force-feedback glove vibrated when touching the virtual object.

Table 5
Comparison with other force-feedback gloves.

Glove	Weight (g)	Stiffness type	Maximum fingertip force (N)	Minimum resistance force (N)	Fingertip number/ finger force feedback	Range of motion	Actuation method	Ref.
Glove in this paper	245	Variable	4	0.1	5	Full hand closing	Pneumatic pump	
CyberGrasp	450	Variable	12	—	5	Full hand closing	Electrical motor	[8]
Wolverine	55	Constant	106	—	4	20–160 mm	Electrical motor	[11]
RMII-ND	20 (per finger)	Variable	7	—	4	—	Pneumatic pump	[13]

This indicates that the stiffness was beyond the capability of the glove.

6. Discussion

The experimental results demonstrate that the proposed solution can produce a small resistance force to simulate the sensation of free space, and can also simulate the sensation of constrained space by providing stable force feedback. As shown in Table 5, the proposed glove is much lighter than the CyberGrasp device, and provides a large range of motion. Compared with the Wolverine glove, the proposed glove provides active force and variable stiffness. Compared with the RMII-ND glove, the actuators and mechanism of the proposed glove are all mounted on the dorsal side, such that the motion range of the fingers is not constrained by the glove. In both free and constrained space, the proposed glove can support full-hand opening and closing.

However, rigorous work must be performed in order to improve the performance of the proposed force-feedback glove. First of all, a major limitation of the proposed physical prototype is that we could not accurately control the magnitude of the normal force perpendicular to the user's fingertip. In order to accurately produce an expected normal force on the fingertip, one possible solution is to introduce a force sensor to formulate a closed-loop control system, and thus to compensate for the error by adjusting the pressure within the pneumatic cylinder in real time.

Second, the responsiveness of the glove should be increased. Compared with the maximal stiffness of typical force-feedback devices such as the PHANTOM Desktop, the maximal stiffness of the proposed glove is much lower. According to the stability theory of haptic devices [18], the maximal stiffness of a haptic device is dependent on the update rate of the sampling and control system. One major reason behind the low maximal stiffness is that the update rate of the proposed glove is too small. As explained in Section 4.2, the propagation velocity of the airflow in the tube caused significant delay. For example, with a tube that was 28 cm long and with an air pressure of 0.54 MPa, the time delay from the electro-pneumatic regulator to the pneumatic cylinder was measured to be 130 ms. In the next step in the development of our device, it will be necessary to find novel solutions to reduce this delay and improve the update rate of the control system.

Third, the proposed solution is not adaptive to different users. A new mechanism needs to be proposed that can adapt to the hand sizes of different users. Furthermore, the mounting structure on the palm is rigid, which gave the users an uncomfortable sensation. Flexible mounting structures need to be developed.

Last but not least, the noise of the pump is rather loud. Solutions such as low-noise pumps or hydraulic actuation methods can be investigated in order to reduce this noise.

7. Conclusions and future work

We developed a force-feedback glove using a lightweight linkage mechanism consisting of only one link for each finger. The total weight of the mechanism on all five fingers is 245 g. The workspace of the five fingers was preserved after mounting the glove. No motion interference occurs for typical grasping motions of the user's hand.

A wearable force-measurement system with a six-axis force/torque sensor was developed in order to measure the equivalent force exerted on the user's fingertip in free-space or constrained-space simulations. The obtained results validated the feasibility of the measurement system for the quantified evaluation of force-feedback gloves.

The experimental results demonstrate that the proposed solution is able to provide free-space sensation by reducing the weight and inertia of the links, and by reducing the joint friction using only four joints on each finger. The average equivalent resistance force is smaller than 0.1 N when simulating free space. A constrained-space sensation is provided using a pneumatic actuation approach. The maximal feedback force is 4 N, and a maximum stiffness of 92 $N \cdot m^{-1}$ with stable force feedback can be simulated.

In the next step, we plan to add miniature force sensors to the mechanism of the glove, and thus achieve closed-loop force control in order to improve the force-feedback accuracy. Furthermore, new control hardware and software need to be constructed in order to increase the bandwidth of the force feedback. Novel application scenarios such as virtual reality based e-shopping could be developed by integrating the glove with a head-mounted display. Finally, we plan to add distributed tactile feedback on the user's palm in order to provide the sensation of contact with virtual objects on the palm area.

Acknowledgements

This work was supported by the National Key Research and Development Program (2016YFB1001200) and the National Natural Science Foundation of China (61572055 and 61633004).

Compliance with ethics guidelines

Yukai Zheng, Dangxiao Wang, Ziqi Wang, Yu Zhang, Yuru Zhang, and Weiliang Xu declare that they have no conflict of interest or financial conflicts to disclose.

Appendix A. Supplementary data

Supplementary data associated with this article can be found, in the online version, at https://doi.org/10.1016/j.eng.2018.10.003.

References

[1] Endo T, Kawasaki H, Mouri T, Doi Y, Yoshida T, Ishigure Y, et al. Five-fingered haptic interface robot: HIRO III. In: Proceedings of the World Haptics 2009 Third Joint Eurohaptics Conference and Symposium on Haptic Interfaces for Virtual Environment and Teleoperator Systems; 2009 Mar 18–20; Salt Lake City, UT, USA. New York: IEEE; 2011. p. 458–63.
[2] Liu L, Miyake S, Akahane K, Sato M. Development of string-based multi-finger haptic interface SPIDAR-MF. In: Proceedings of the 2013 23rd International Conference on Artificial Reality and Telexistence; 2013 Dec 11–13; Tokyo, Japan. New York: IEEE; 2014. p. 67–71.

[3] Winter SH, Bouzit M. Use of magnetorheological fluid in a force feedback glove. IEEE Trans Neur Syst Rehabili Engine 2007;15(1):2–8.
[4] Blake J, Gurocak HB. Haptic glove with MR brakes for virtual reality. IEEE/ASME Trans Mechatron 2009;14(5):606–15.
[5] Tadano K, Akai M, Kadota K, Kawashima K. Development of grip amplified glove using bi-articular mechanism with pneumatic artificial rubber muscle. In: Proceedings of the 2010 IEEE International Conference on Robotics and Automation; 2010 May 3–7; Anchorage, AK, USA. New York: IEEE; 2010. p. 2363–8.
[6] Ho NSK, Tong KY, Hu XL, Fung KL, Wei XJ, Rong W, et al. An EMG-driven exoskeleton hand robotic training device on chronic stroke subjects: task training system for stroke rehabilitation. In: Proceedings of the 2011 IEEE International Conference on Rehabilitation Robotics; 2011 Jun 29–Jul 1; Zurich, Switzerland. New York: IEEE; 2011. p. 5975340.
[7] Nam AYJ, Park MK, Yamane R. Smart glove: hand master using magnetorheological fluid actuators. Proc SPIE 2007;6794:679434.
[8] Cybergrasp [Internet]. San Jose: CyberGlove Systems LLC, Inc.; c2017. [cited 2018 Mar 12]. Available from: http://www.cyberglovesystems.com/.
[9] 3D System [Internet]. Inc.; c2018. [cited 2018 Mar 12]. Available from: https://www.3dsystems.com/haptics-devices/geomagic-touch-x/specifications.
[10] Koyama T, Yamano I, Takemura K, Maeno T. Multifingered exoskeleton haptic device using passive force feedback for dexterous teleoperation. In: Proceedings of the IEEE/RSJ International Conference on Intelligent Robots and Systems; 2002 Sep 30–Oct 4; Lausanne, Switzerland. New York: IEEE; 2002. p. 2905–10.
[11] Choi I, Hawkes EW, Christensen DL, Ploch CJ, Follmer S. Wolverine: a wearable haptic interface for grasping in virtual reality. In: Proceedings of the 2016 IEEE/RSJ International Conference on Intelligent Robots and Systems; 2016 Oct 9–14; Daejeon, South Korea. New York: IEEE; 2016. p. 986–93.
[12] Walairacht S, Ishii M, Koike Y, Sato M. Two-handed multi-fingers string-based haptic interface device. IEICE Trans Inf Syst 2001;84:365–73.
[13] Bouzit M, Burdea G, Popescu G, Boian R. The Rutgers Master II-new design force-feedback glove. IEEE/ASME Trans Mechatron 2002;7(2):256–63.
[14] Zubrycki I, Granosik G. Novel haptic glove-based interface using jamming principle. In: Proceedings of the 2015 10th International Workshop on Robot Motion and Control; 2015 Jul 6–8; Poznan, Poland. New York: IEEE; 2015. p. 46–51.
[15] Polygerinos P, Wang Z, Galloway KC, Wood RJ, Walsh CJ. Soft robotic glove for combined assistance and at-home rehabilitation. Robot Auton Syst 2015;73(C):135–43.
[16] Kang BB, Lee H, In H, Jeong U, Chung J, Cho KJ. Development of a polymer-based tendon-driven wearable robotic hand. In: Proceedings of the 2016 IEEE International Conference on Robotics and Automation; 2016 May 16–21; Stockholm, Sweden. New York: IEEE; 2016. p. 3750–5.
[17] Force Dimension [Internet]. Switzerland: Force Dimension, Inc.; c2001–2018. [cited 2018 Mar 12]. Available from: http://www.forcedimension.com/products.
[18] Colgate JE, Schenkel GG. Passivity of a class of sampled-data systems: application to haptic interfaces. In: Proceedings of the 1994 American Control Conference-ACC'94; 1994 Jun 29–Jul 1; Baltimore, MD, USA. New York: IEEE; 2002. p. 3236–40.